International Journal of Biological Macromolecules 210 (2022) 94–106

Contents lists available at ScienceDirect

International Journal of Biological Macromolecules

journal homepage: www.elsevier.com/locate/ijbiomac

Preparation of chitosan/tannin and montmorillonite films as adsorbents for Methyl Orange dye removal

Nadia Tahari [a,b,c], Pedro L. de Hoyos-Martinez [c], Nagore Izaguirre [c], Nefzi Houwaida [a,b,c], Manef Abderrabba [b], Sameh Ayadi [d], Jalel Labidi [c,*]

[a] University of Tunis El Manar, Faculty of Sciences of Tunis, B.P: 248, El Manar II, 2092 Tunis, Tunisia
[b] Laboratory of Materials, Molecules and Applications, IPEST, Preparatory Institute of Scientific and Technical Studies of Tunis, University of Carthage, Sidi Bou Said road, B. P.512070, La Marsa, Tunisia
[c] Biorefinery Processes Research Group, Department of Chemical and Environmental Engineering, University of the Basque Country (UPV/EHU), Plaza. Europa1, 20018 Donostia-San Sebastian, Spain
[d] Laboratory of Materials, Treatment and Analysis, INRAP, Technopôle Sidi-Thabet, Tunis 2020, Tunisia

ARTICLE INFO

Keywords:
Chitosan
Tannin
Montmorillonite
Films
Methyl orange
Adsorption mechanism

ABSTRACT

A series of novel chitosan/tannin/montmorillonite (Cs/Tn/MMT) films were synthesised by loading different (from 0.2 to 0.5 wt%) and MMT (from 0.5 to 1.5 wt%) ratios, to be used as promising low-cost biosorbents for methyl orange (MO) removal from aqueous media. The prepared films were characterised using different techniques such as x-ray diffraction (XRD), Fourier transform infrared spectroscopy (FTIR), water contact angle, optical properties, colourimetric measurement, porosity, swelling and thickness. The effects of various parameters, i.e. initial MO concentration, adsorbent dose, pH and temperature, were studied. The Cs/Tn0.2/MMT1 film showed a high removal efficiency of 95.62% and maximum adsorption capacity of 57.37 mg/g under the optimum adsorption conditions (initial methyl orange concentration 60 mg/L, pH 7 and 25 °C). The adsorption kinetic followed the pseudo second order kinetic model and the experimental data were a good fit for the Langmuir isotherm indicating a homogeneous and monolayer adsorption process. The thermodynamic parameters suggested physical adsorption and exothermic behaviour. Consequently, Cs/Tn/MMT films showed effective potential for the uptake of anionic dyes.

1. Introduction

Water contamination with synthetic dyes is a serious issue, which can produce significant damage to the planet and cause severe problems to human health. In fact, dyes are classified as highly polluting, carcinogenic and toxic elements [1]. Methyl Orange (MO) is an anionic dye that belongs to the azo group and presents a type of p-amino azobenzene (p-AAB) [2]. This compound has been extensively used for a variety of applications in the pharmaceutical, printing, food, paper, and textile industries, as well as in research laboratories as an acid-base indicator [3]. This intense pigment is toxic and poses a serious threat to the lives of animals and human health, to the point where it can cause, vomiting, diarrhea and even death, after a high exposure [4]. Within the conventional techniques used for wastewater treatment, adsorption is the most common approach in reducing the hazards derived from harmful compounds, due to the short time and simplicity of operations, high efficiency and wide availability of adsorbents [5].

Clay has been one of the most common biological adsorbents used for wastewater treatment applications over the years [6] and it can be combined with other biopolymers, such as lignin [7], chitosan [8–11] and starch [12].

Chitosan (Cs) has a great potential for use as an adsorbent for dye

Abbreviations: MMT, Montmorillonite; Cs, Chitosan; Tn, Tannin; MO, Methyl Orang; C_0, Initial MO concentration (mg/L); C_e, Concentration of MO solution at equilibrium (mg/L); q_e, Amount of MO adsorbed at equilibrium (mg/g); q_t, Amount of MO adsorbed at time (t) (mg/g); K_1, The constant adsorption pseudo-first-order model (min^{-1}).; K_2, The constant adsorption pseudo-second- order model (g mg^{-1}/min); $Q_{e,\ cal}$, Amount of MO calculated at equilibrium (mg/g); $Q_{e,\ exp:}$, Amount of MO of the experimental at equilibrium (mg/g); K_F, Freundlich adsorption isotherm constant (mg/g); $\frac{1}{n}$, Freundlich adsorption isotherm constant; K_L, Langmuir isotherm constant (L mg^{-1}); Q_m, The maximum adsorption capacity (mg/g); T, Temperature (°C, K); KT, Temkin constant; KDR, Dubinin-Radushkevich (R-D) constant; AT, Equilibrium binding constant; E, Free Energy.

* Corresponding author.
E-mail address: jalel.labidi@ehu.es (J. Labidi).

https://doi.org/10.1016/j.ijbiomac.2022.04.231
Received 26 September 2021; Received in revised form 3 April 2022; Accepted 30 April 2022
Available online 4 May 2022

removal, owing to its non toxicity, biodegradability, biocompatibility, chelating capability, low price and availability [13]. The amino ($-NH_2$) and hydroxyl (-OH) groups present in its structure provide a polycationic singular nature, which ameliorates the active adsorption sites toward pollutant removal [14]. Chitosan is a linear biopolymer comprising amino polysaccharide units such as D-glucosamine and *N*-acetyl-D-glucosamine, which is obtained by the alkaline *N*-deacetylation of chitin, one of the most abundant polysacharides found in nature [15]. It shows great potential in diverse fields, such as medicine [16], agriculture [17], food packaging [18] and biochemistry. In recent years, Cs-immobilised montmorillonite (MMT) has been studied as an important combination for enhancing the chemical properties and improving the removal efficiency of dye [10,19].

Likewise, tannins represent one of the most important families of biopolymers, with important applications and availability in nature. Tannins display an aromatic structure, with high amounts of carboxyl and hydroxyl groups [20]. The repetition of these units provides tannins with important characteristics, such as their crosslinking capacity, high purity and reactivity [21]. These molecules are mainly derived from plant and wood bark, as well as seeds and roots. One of the most common feedstocks of tannins, especially of the condensed type, is *Acacia Mearnsii*. Concerning their application as adsorbents, the use of raw and immobilised tannins for wastewater treatment has been reported by various authors; for example, their adsorption effects toward cationic and anionic dyes have been studied [22,23].

Several studies have reported on the combinations and synergy effects between the previously introduced compounds, i.e. montmorillonite, chitosan and tannins. Thus, the integration of montmorillonite with tannins was used for pollutant removal [24–26]. In addition, it has been reported that the biomaterials based on tannin and chitosan performed well in the adsorption of dyes in [27,28]. In [29], Tannin/chitosan/sericite microcapsules were employed as low-cost, highly efficient bioadsorbents for the removal of Pb (II), due to the presence of hydroxyl, carboxyl, carbonyl and amino groups in their structure.

There has been an increased focus on biopolymer films as good adsorbents for wastewater treatment [30]. In this respect, the important number of active sites is a major advantage for the adsorption of many types of water pollutants [31,32]. For instance, Bapun Barik et al. reported the alumina-based, crosslinked chitosan-HPHC biocomposite film enhanced the removal of fluoride and azo dye [33]. In another study, Fe-loaded chitosan films presented a greater chemical stability and adsorption capacity for MO removal than pristine Cs, which can achieve 205 mg/g [34]. Laysandra et al. prepared a composite film, based on chitosan, saponin and bentonite, for methyl orange and chromium removal [35]. The results indicated that the high adsorption capacity achieved for CSB2:3 was 360.90 mg/g at 60 °C. Therefore, this is the first work that has dealt with a combination of montmorillonite clay, chitosan and mimosa tannins for the elaboration of films for dye removal from wastewater.

The objective of the current work is to introduce a new eco-friendly and cost-effective process, for the synthesis of chitosan films with immobilised tannin and montmorillonite, to facilitate the adsorption of MO from aqueous media. Various amounts of MMT (0.5, 1.0, 1.5 and 2.0 wt%) and Tn (0.2, 0.3, 0.4 and 0.5 wt%) were added to the chitosan matrix. The resultant products were characterised structurally and chemically. Adsorption batch experiments, considering the initial dye concentration, adsorbent doses, pH and temperature, were performed to determine the factors that affect the removal efficiency. Adsorption kinetics and models were also investigated.

2. Experimental

2.1. Materials

Montmorillonite K10 (MMT), acetic acid, ethanol and methyl orange (MO) were purchased from Sigma-Aldrich. Microcrystalline chitosan powder (with a degree of deacetylation of 98% and Mw 500,000 g/moL) was purchased from Mahtani Chitosan Pvt. Ltd., India. Commercial tannin (Tn) extracted from mimosa (*Acacia mearnsii*), with the label 'Tanfood', was kindly provided by TANAC S.A. (Brazil). This product is classified as condensed tannin and it displays a high reactivity (Stiasny number ≈90%). The mimosa tannin has a high purity, with a 97% content of organic compounds and a molecular weight of 3402 g/mol. All chemical reagents were used without further purification. Deionized water was used in all of the experiments.

2.2. Preparation of Cs/Tn/MMT films

The films based on Cs, Tn and MMT were prepared in three steps via a solvent casting method using circular-shaped moulds. This procedure consisted of the dispersion of the biopolymer in an adequate solution, followed by the evaporation of the solvents [36]. The procedure described by Zhang was followed with some modifications [37]. Firstly, 1% (*w*/*v*) chitosan solution was prepared by dissolving 1 g of Cs in 100 mL of 1% (*v*/v) acetic acid solution under continuous magnetic stirring at room temperature until dissolution (Solution I). Secondly, different amounts of tannin (namely 0.2, 0.3, 0.4 and 0.5 wt%) were dispersed in 1% (*v*/v) of acetic acid and left with magnetic stirring for 2 h (Solutions II). Thirdly, the appropriate amount of MMT was separately dispersed in distilled water in an ultrasound bath at 50 °C for 2 h and 240 W, to enhance the subsequent exfoliation process [38]. The MMT dispersions were prepared at different proportions, i.e. 0.5, 1.0, 1.5 and 2.0 wt% (Solutions III).

Finally, solutions I, II and III were mixed in the same proportions. The amounts of chitosan, tannin and montmorillonite used for the preparation of the different film formulations are summarised in Table 1. The mixtures were stirred for 2 h at 9000 rpm and 50 °C to obtain a uniformly dispersed Cs, Tn and MMT solution. Once this was achieved, the mixture was cast into silicone moulds and dried in an incubator at 30 °C for 5 h.

The obtained films from the previous procedure are presented in Fig. 1. The resultant films are flexible and brown-coloured due to the presence of tannins. As the content of both tannins and montmorillonte was increased, the films obtained became more brittle. The morphology and adsorbent properties of these films are presented in the following section.

2.3. Physicochemical characterisation of the films

2.3.1. X-Ray diffraction study (XRD)

X-ray diffraction measurements were performed to investigate the incorporation process of the different components of the films and their influence in the structure. Diffraction scatters were collected with a Panalytical X'Pert PRO diffractometer (Almelo, the Netherlands) with a Cu Kα radiation (λCuKαmedia = 1.5418 Å, λCuKα1 = 1.54060 Å and λCuKα2 = 1.54439 Å) in the 2θ range from 3° to 70°.

2.3.2. Fourier Transform Infrared (FTIR) Spectroscopy

Fourier transform infrared spectroscopy (FTIR) measurements were carried out on a Perkin-Elmer Spectrum Two FT-IR Spectrometer,

Table 1
Tannin and montmorillonite composition of the films.

Samples	Chitosan	Tannin (%)	Montmorillonite (%)
Cs/Tn0.2/MM0.5	+	0.2	0.5
Cs/Tn0.3/MMT0.5	+	0.3	+
Cs/Tn0.4/MMT0.5	+	0.4	+
Cs/Tn0.5/MMT0.5	+	0.5	+
Cs/Tn0.2/MMT0.5	+	0.2	0.5
Cs/Tn0.2/MMT1	+	+	1
Cs/Tn0.2/MMT1.5	+	+	1.5
Cs/Tn0.2/MMT 2	+	+	2

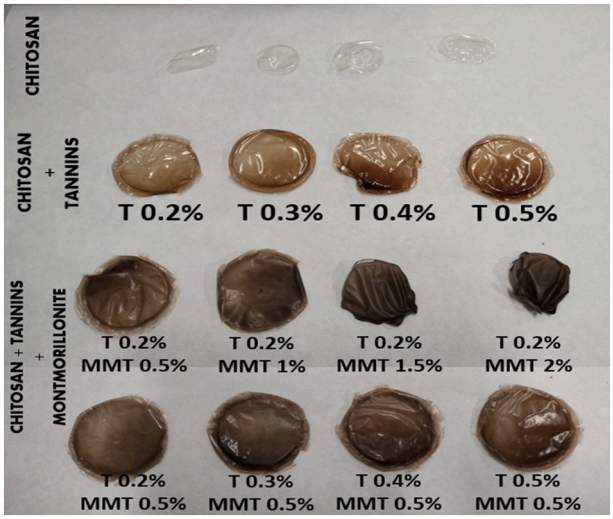

Fig. 1. Digital images of the brittle Cs, Cs /Tn and Cs/Tn/MMT films with different tannin and montmorillonite proportion.

equipped with a L1050231 Universal Attenuated Total Reflectance (ATR) accessory (Perkin-Elmer, USA). Each sample analysis was carried out in transmittance mode, with 64 scans being accumulated in a transmission mode at a resolution of 4 cm^{-1} from a range of 4000–400 cm^{-1}.

2.3.3. Water contact angle (CA) measurement

The contact angle (CA) was measured with a Dataphysics Contact angle system OCA 20, to determine the changes in the hydrophilic character of the films and the influence of the different components on this parameter. Uniform strips were used for this purpose. To examine the water repellence of composites, water was used by the placement of a droplet (5 μL). An average value of five measurements per sample was calculated; the values being expressed as means ±standard deviation.

2.3.4. Optical properties

The optical properties of the films were measured using a UV–vis spectrophotometer (Jasco V-730 spectrophotometer). Each film was scanned from 200 to 800 nm and the transmittance values were obtained. From each film type, three different sections were scanned.

2.3.5. Colourimetric measurement

The colour of the films obtained was measured by the determination of the different parameters: L* for lightness, a* for greenness (from green to red), b* for yellowness (from blue to yellow), ΔC* for chroma difference, Δh* for hue difference, and ΔE* for the overall colour difference. The colourimeter used was a PCE-CMS 7 from PCE Instruments (Spain). A standard white plate was used as a baseline and mean values of the five measurements from each film were used.

2.3.6. Porosity measurement

The percentage of film porosity was measured using a liquid displacement method. Ethanol was selected as the displacement liquid. This method consisted of immersing the different dried film formulations in absolute ethanol for 24 h. Once equilibrium was reached, the films were removed and the weight of residual ethanol was recorded [39]. The porosity of the films was calculated using the following equation:

$$\text{Porosity}\ (\%) = \left[\frac{W_2 - W_1 - W_3}{W_2 - W_3}\right] \times 100 \quad (1)$$

W_1 is the weight of the film, W_2 is the sum of the ethanol and the immersed film and W_3 is the weight of residual ethanol after removal of the film. An average value of three measurements was calculated per sample.

2.3.7. Swelling/water adsorption measurement

The swelling or water adsorption properties were measured after immersing the prepared films separately into saline solution at room temperature [39,40]. The soaked films were withdrawn at different time intervals (1, 3 and 5 h) and the swelling weight value was determined after filtering the film with a filter paper to remove excess surface water. Then, the films were placed into the same solution and the swelling percentage was calculated according to the following equation:

$$\text{Swelling}\ (\%) = \left[\frac{W_4 - W_1}{W_1}\right] \times 100 \quad (2)$$

W_1 is the weight of the dried film and W_4 is the weight of the wet film at different time intervals. An average value of three measurements was calculated per sample.

2.3.8. Thickness measurement

The thickness of the prepared films was measured with the screw gauge method. Five positions of each film were randomly measured and the average ± standard deviation recorded [40,41].

2.4. Assessment of the adsorption of the films

To investigate the performance of the films for the adsorption of methyl orange dye (MO), a solution of MO dye was prepared by dissolving 0.1 g of MO powder in 100 mL of distilled water, which was stirred vigorously at 100 rpm for 80 min. From this pristine solution, aliquots of diluted concentrations were prepared for the different adsorption analysis (according to the desired concentration of MO in each case). The dosage of the dye was spectrophotometrically performed every 5 min, at 500 nm (taken as the maximum wavelength using the Jasco-V-630 Spectrophotometer). The adsorption capacity (q_e) and the percentage of adsorption (%R) were calculated using Eqs. (3) and (4):

$$q_e = \frac{(C_0 - C_e)V}{m} \quad (3)$$

$$\%R = \left(\frac{C_0 - C_e}{C_0}\right) \times 100 \quad (4)$$

where q_e is the capacity of adsorption at equilibrium (mg/g), C_0 and C_e are the initial and the equilibrium concentration (mg/L), m is the amount of adsorbent (g) and V is the volume of the solution (L).

To investigate the adsorption process, a kinetic study was carried out. Within this study, different parameters were evaluated: the MO concentration was varied in the range 20 to 60 mg/L, the pH was varied in the range 2–11, and the amount of MMT and tannin were varied in the range 0.5–2.0%. and 0.2 to 0.5%, respectively.

3. Results and discussion

3.1. Characterisation of films

3.1.1. XRD analysis of the films

This technique was carried out to assess the structural changes derived from the addition of the different raw materials. The diffractograms of Cs/Tn and Cs/Tn/MMT films, as well as the separated diffractograms of the raw materials (Cs, Tn and MMT) are shown in Fig. 2.

Chitosan displayed a semicrystalline structure, with three sharp signals at $2\theta = 8.61°$, $11.69°$ and $18.48°$, corresponding to the crystalline phase [42]. This biopolymer presents a broad halo pics around $2\theta = 23.35°$, corresponding to the amorphous phase [43]. According to a recent study by Weijie Lan et al., the peak of Cs at 23.35° disappeared in the Cs films, which is attributed to the formation of an amorphous state

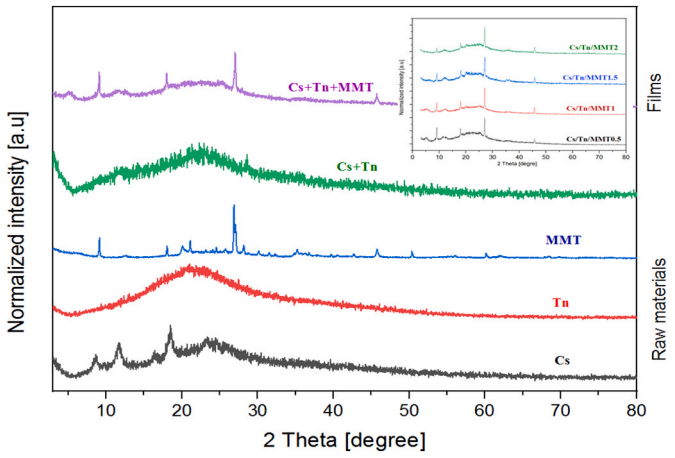

Fig. 2. X-Ray Diffraction Spectra of raw materials and the Cs/Tn/MMT films formulations.

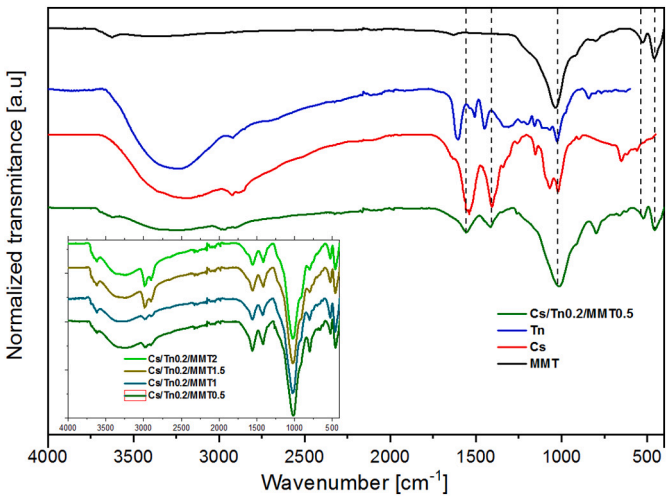

Fig. 3. Fourier Transform Infrared Spectra of raw materials and all the Cs/Tn/MMT films formulations.

in the film structure [44]. The signal at 11.52° was related to the hydrated conformation of chitosan [45]. The spectra of tannin showed a halo at 2θ = 20.39°, which is typical for an amorphous structure [46]. Montmorillonite presents high crystalline structure, characterised by several peaks. In the region of 2θ = 0–10°, a moderate to high intensity signal was observed at 9°; in the region of 2θ = 10–30°, moderate to low signals at 18°, 20°, and 21°, and a high intensity signal at 27° were associated with the crystalline plane of quartz. In the last region, 2θ = 40–80°, the most significant signal was found at 46° [47].

The diffractogram of the Cs/Tn films showed a prominently amorphous structure, where the signals typical of the crystalline part of chitosan (2θ = 8.61° and 11.69°) appeared to be attenuated. The same behaviour was observed for the halo signals of Cs and Tn.

The Cs/Tn/MMT films presented an increase in the crystallinity of their structure, as a consequence of the introduction of the MMT clay. In fact, the intensity of the amorphous phase of Cs and Tn was considerably decreased, which might be attributed to the role of the compensation cations of MMT present during the modification, which could hinder the coordination of Tn [48]. On the one hand, the peaks at 2θ = 9°, 18°, 27°, and 46° corresponded to the crystal diffraction phases of MMT but, on the other hand, the crystalline signals of Cs at 2θ = 8.61°, 11.69°, and 18.48° were also found. At 2θ = 9° and 18°, the double contribution of Cs and MMT resulted in a higher intensity compared to that of the raw material. Considering these two peaks, the concentration of MMT in the film and the intensity of these signals were correlated inversely. At low MMT concentration (0.5 wt%), a good interaction and exfoliation of the MMT layers with chitosan in the films was achieved. The results also show a decrease of the (001) plane intensity, which is detected at 7.8° for Cs/Tn/MMT0.5 and Cs/Tn/MMT2, followed by a shift in the diffraction angle. Babul Reddy et al. concluded that this result can be indicative of the co-existence of a good interaction and exfoliation of MMT layers in chitosan-PAV nanocomposite films [49]. However, as the MMT concentration increased, the interaction between these phases decreased, resulting in visible segregation in the final appearance of the films. The platelets of clay layers can be exfoliated between them, to form a film structure [50]. This exfoliation can be noted via XRD and FTIR analysis. In this respect, the disappearance of the characteristic diffraction peak of clay at 19.8° in the Cs/Tn/MMT structure can be explained by the increase of d-spacing. This would indicate good exfoliation of MMT layers.

3.1.2. *FTIR analysis of the films*

FTIR analysis of the raw materials and films was performed, to evaluate the contribution of each pristine component (Cs, Tn and MMT) and the structure of each film (Fig. 3).

First of all, chitosan displayed a broad band between 3500 and 3000 cm^{-1} which is related to the O—H and N—H stretching vibration [51]. Between 3000 and 2800 cm^{-1}, two medium-low intensity signals were observed, associated with CH_2 stretching of chitosan and the O—H [35]. At 1550 cm^{-1} and 1405 cm^{-1}, two sharp signals were detected, corresponding to amine groups and C—H bending vibration, respectively. In the last section of the spectra, an intense band of C—O vibrations appeared with two signals, the first at 1075 cm^{-1} (of primary alcohol) and the second at 1014 cm^{-1} (of ether bonds) [52].

On the other hand, the tannin spectra presented the same signals associated with hydroxyl and methylene groups, observed between 3500 and 3000 cm^{-1}. Between 1600 and 1450 cm^{-1}, medium intensity signals were detected and attributed to aromatic ring stretching vibrations. In the range 1300–1000 cm^{-1}, the signals were related to C-O-C stretching of pyran heterocyclic rings, which is typical of flavonoids [53].

As seen in the FTIR spectrum, MMT shows a characteristic peak at 3624 cm^{-1} and 3300 cm^{-1} which are attribued to the stretching vibration of Al-OH, Si-OH, O—H, and H-O-H groups [40]. In the spectrum, three peaks were highlighted: one peak, with its highest intensity at 1040 cm^{-1}, was related to Si-O-Si symmetric stretching, and two others were moderate-low intensity (at 520 and 460 cm^{-1}) and attributed to Si-O-Al linkages and deformation of Si-O-Si bonds, respectively [54]. These pics were associated with the montmorillonite spectra.

The film spectra first presented a small peak at 3600 cm^{-1}, which corresponded to the stretching vibration of OH groups from Cs and Tn associated with octahedral cations of MMT [55]. The region between 3500 and 3000 cm^{-1} was associated with the total -OH and -NH of the montmorillonite and chitosan components and presented a lower intensity, compared to the spectra of pristine Tn and Cs. This is due to the interaction and crosslinking of these components with MMT through this functional group [52]. A significant peak of Si—O vibration of MMT, at 1015 and 522 cm^{-1}, was observed in Cs/Tn/MMT (1–2%) spectra [49]. Daniela Enescu et al. reported that the shift of the stretching vibration of SiO_2 in the film spectra from 1035 cm^{-1} to 1015 cm^{-1} could be the result of the hydrogen band interaction between the chitosan structure and montmorillonite layers [56]. The peak with the highest intensity (observed at 1020 cm^{-1}) was attributed to the combination of Si-O-Si from MMT and the C—O from Cs and Tn (overlapped). The significant peak at 522 cm^{-1} designed the Si—O vibration of MMT were observed in Cs/Tn/MMT (1–2%) spectra [49]. The two signals detected in the region at 520 and 460 cm^{-1} of MMT were also present in the structure of the films, confirming the proper introduction of MMT into the organic polymeric matrix of Cs-Tn. It was highlighted that increments of the MMT concentration led to the increase of the signals at

3600, 2900, and 2800 cm^{-1}. On the contrary, the typical Cs signals at 1560 and 1400 cm^{-1} were significantly reduced as the proportion of MMT was higher.

3.1.3. Water contact angle

The contact angle (θ_c) was determined to evaluate the influence of tannin and montmorillonite on the hydrophilic character of the prepared films. The results are shown in Fig. 4 and they correspond to the mean values of this parameter, measured at $t = 0$ s.

Compared to the reference films (Cs only), the introduction of tannin resulted in an increment of wettability of the films, i.e. higher hydrophilicity (<90°). Thereby, the θ_c was greatly reduced from 99.80 ± 3.95° (for the reference Cs film) to 75.45 ± 1.63° (for the Cs/Tn 0.5 w% film). As seen in other studies, this was derived from a greater concentration of the polar polyphenolic groups inherent to the tannin structure [57–59]. The effect of tannin concentration at a fixed MMT concentration (0.5 wt%), was also studied. The same tendency was remarked upon, after the introduction of 0.5 w% of MMT in the Cs/Tn films; a decrease of the θ_c from 72.13 ± 5.05° (for Cs/Tn0.2/MMT0.5) to 67.45 ± 0.21° (for Cs/Tn0.5/MMT0.5). Considering the pursued application of dye removal from water, a lower concentration of MMT would be more convenient, owing to the necessity of a certain hydrophilic character [60].

Cs/Tn0.2/MMT1 presented a lower contact angle than Cs/Tn0.2, which indicated that an increase of 1w% of MMT concentration also increases the wetability of the films. The increase of MMT led to a lower wettability of the films (θ_c = 89.16° ± 5.5, for Cs/Tn0.2/MMT1.5 to θ_c = 94.73° ± 3.56, for Cs/Tn0.2/MMT2) which proved the formation of particle aggregation at higher MMT content (more than 1.5w%). This tendency was associated with a reduction of the polar groups in the surface, as reported by Chen et al. [60]. This is also in accordance with the results obtained in the previous section, in which the band attributed to hydroxyl groups was reduced.

3.1.4. Optical properties of the films

The films were scanned with a UV–vis spectrophotometer to analyse the transmittance of the radiation, taking into account their constituents. The spectra of the different films are presented in Fig. 5. First, it was observed that the films with Tn and MMT exhibited good UV light (200–400 nm) barrier properties compared to the reference film (Cs). With regards to the visible range (400–700 nm), it could be seen that these reference films were highly transparent, with a high percentage of transmittance values. The addition of tannin to the films resulted in a considerable reduction of the transmittance in this range, between 45.3% and 65.9% at 700 nm, and 15.0% and 22.0% at 400 nm. This same tendency was reported by Panpan Li et al., indicating that tannin is able to absorb 92% of UV light when the wavelength is below 320 nm [61]. Since the Cs/Tn films displayed a red-brownish colour inherent to tannin, the transmittance values at the end of the visible spectra (typically red wavelengths) were higher than those from the beginning of this range (typically blue wavelengths). In the Cs/Tn/MMT films, the introduction of this last constituent led to a severe decrease of transmittance. Considering CS, a reduction of 75% at 400 nm and 82–85% at 700 nm was observed. The addition of MMT could change the transparency of the film to opaque [62]. On the other hand, at a fixed tannin concentration, the increase in the MMT percentage only resulted in a slight reduction of the transmittance. This same tendency could be seen when the MMT concentration was set and the contribution of tannin was raised.

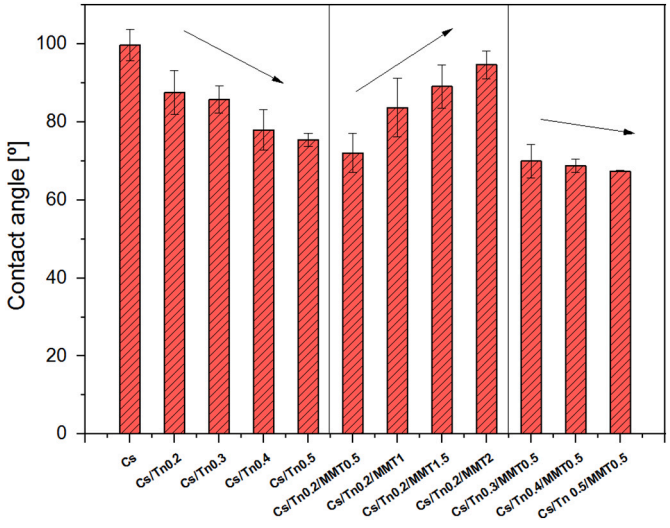

Fig. 4. Contact angle values of Cs and Cs/Tn/MMT films with different Tn and MMT contents. The error bars represent standard deviations.

3.1.5. Colourimetric analysis of the films

Changes in the colour parameters of the films are represented in Fig. 6. The parameters measured were L* for lightness, a* for greenness (from green to red), b* for yellowness (from blue to yellow), ΔC* for chroma difference, Δh* for hue difference, and ΔE* for the overall colour difference. Considering Δa*, it was observed that the increase of the Tn percentage led to higher values of this parameter in all of the formulations. In fact, the darker colour of the films indicated a higher tannin concentration [59]. This behaviour was expected due to the typical red-brown colour of tannins, as mentioned in the previous section. The difference observed in Δb* was more significant in the films where MMT was not present, since this component decreased the level of yellowness. In this respect, it has been reported in the literature that an increase of the Tn concentration causes a higher level of yellowness [44]. The variations in the ΔC* parameters were influenced by the presence of Tn and MMT. The former component provided brighter films, whereas, the other led to duller films. The ΔH* parameter was not influenced by either of the film components. The incorporation of Tn and MMT changed the ΔE* values significantly. Besides this, the increase of the ΔE* of the films showed that the incorporation of tannin and montmorillonite increased the opacity and the brownish colour, owing to the addition of a crosslinking agent [57]. However, the variations in their percentages only made a slight difference to this parameter, especially in the case of MMT. Lastly, the lightness variation (ΔL*) displayed a negative tendency, meaning that the films with Tn and MMT presented a darker colour. Yasemin Kasirga et al. observed that the decrease of the L* and a* values and the increase of the b* value could be the reason for the formation of nanoparticle aggregation, which can obstruct light transmission after the addition of MMT K10 into chitosan films [63].

3.1.6. Porosity of the films

In general, the majority of the film formulation showed high porosity (Table 2), since the values were in the range from 85.03 to 92.77%. The porosity of the chitosan films (Cs) decreased from 91.84 to 90.67% with the addition of tannin (0.2%), while this parameter increased from 91.84 to 92.77% with the addition of montmorillonite (0.5%). The same tendency was reported by Dutta et al., who indicated that the porosity of pure chitosan increased with the addition of sepiolite [39]. It was seen that an increase in the amount of tannin (from 0.2 to 0.5%) had no significant influence on the porosity of the films. On the other hand, an increase in the amount of MMT (from 0.5 w% and 1 w%) increased the porosity of the Cs/Tn0.2 film. This behaviour indicated that the addition of montmorillonite (more than 1.5 w%) reduces this parameter.

3.1.7. Swelling ratio of the prepared films

The swelling percentage of the prepared films is an important parameter, which can give a good indication of the porous and hydrophilic structure. As shown in Fig. 7 (a), the swelling percentage

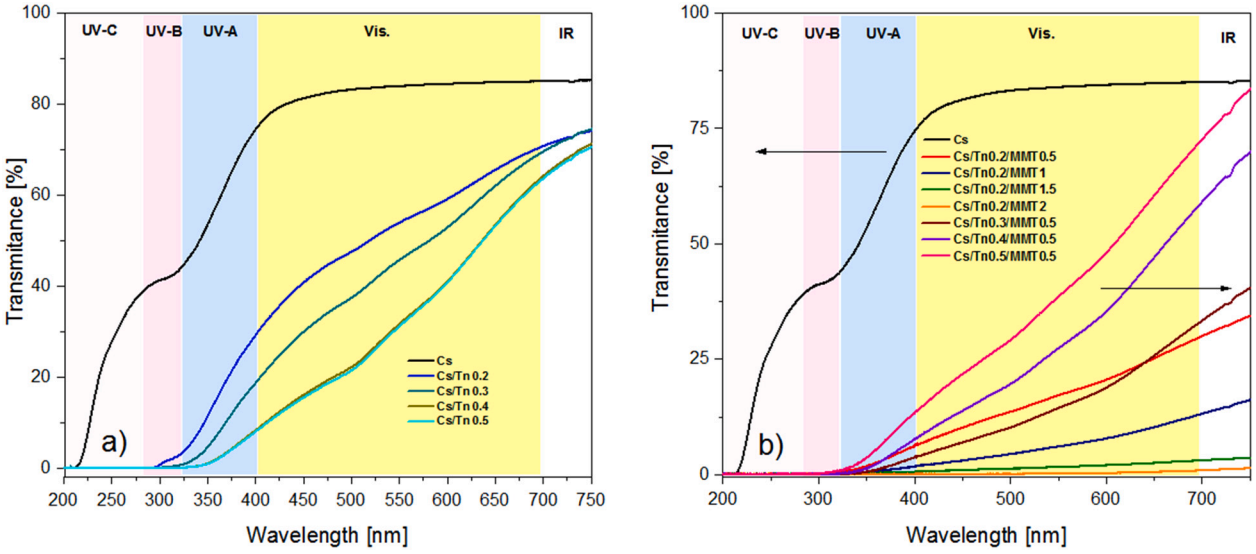

Fig. 5. Transparency analysis of the films.

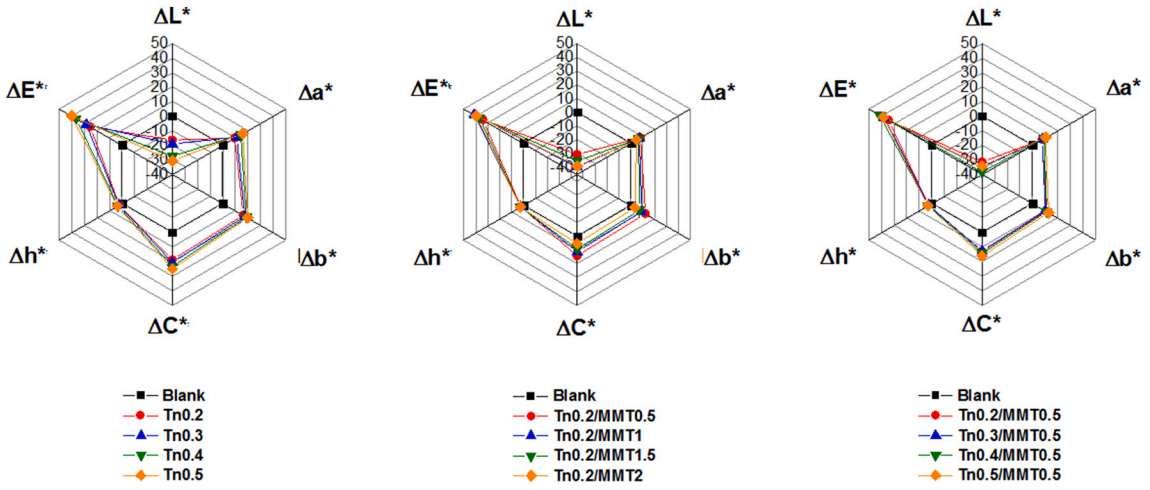

Fig. 6. Colour's parameters of the films.

Table 2
Porosity properties of the films. Values are expressed as mean ± standard deviation.

Films	Porosity (%)
Cs	91.84 ± 3.89
Cs/Tn0.2	90.67 ± 2.19
Cs/Tn0.3	91.17 ± 1.03
Cs/Tn0.4	89.40 ± 2.30
Cs/Tn0.5	90.23 ± 7.15
Cs/Tn0.2/MMT0.5	89.70 ± 2.01
Cs/Tn0.3/MMT0.5	92.33 ± 2.07
Cs/Tn0.4/MMT0.5	90.67 ± 1.69
Cs/Tn0.5/MMT0.5	90.80 ± 6.49
Cs/MMT0.5	92.77 ± 1.93
Cs/Tn0.2/MMT1	91.37 ± 3.62
Cs/Tn0.2/MMT1.5	87.11 ± 5.57
Cs/Tn0.2/MMT2	85.03 ± 1.54

increased with increasing MMT content, from 0.5w% to 2w% (from 31.82 ± 13.64% to 539.39 ± 35.7%) and Cs/Tn0.2/MMT2 displayed the highest swelling properties among all the prepared films. These results are in agreement with other published work, indicating that the hydrophilic character of montmorillonite influences the water absorption capacity [40]. Babul et al. showed that the highest swelling capacity was attributed to the highest MMT content, due to the intermolecular interaction between water molecules in clay galleries and the (-NH_2, -OH) groups present in Cs-PVA chain films [49]. On other hand, Tn content decreases the swelling properties of the Cs/Tn/MMT0.5 films (at a fixed 0.5w% MMT), as shown in Fig. 7 (b). Peña et al. reported that the reduction of swelling values with increased tannin content in a gelatin film matrix is probably due to the presence of high hydrogen interactions, which decrease the number of polar chain groups to uptake and bind water molecules [46].

3.1.8. *Thickness measurement of the prepared films*

The thickness measurement values of all the film formulations that were prepared, are shown in Table 3. The results indicated that the thickness of all the formulations were in the range 31.0 ± 5.0 to 54.2 ± 14.9 μm. Cs films presented the highest thickness values. The addition of tannin resulted in a decreasing tendency in the thickness values, whereas the addition of MMT presented an increasing tendency in the thickness values, from 40.8 ± 10.8 to 54.2 ± 14.9 μm (Cs/Tn0.2/MMT0.5 to Cs/Tn0.2/MMT2). This result suggests that MMT content influences the hardness of the Cs film and Tn influences the thickness of the film. This may be due to incomplete dispersion or aggregation and

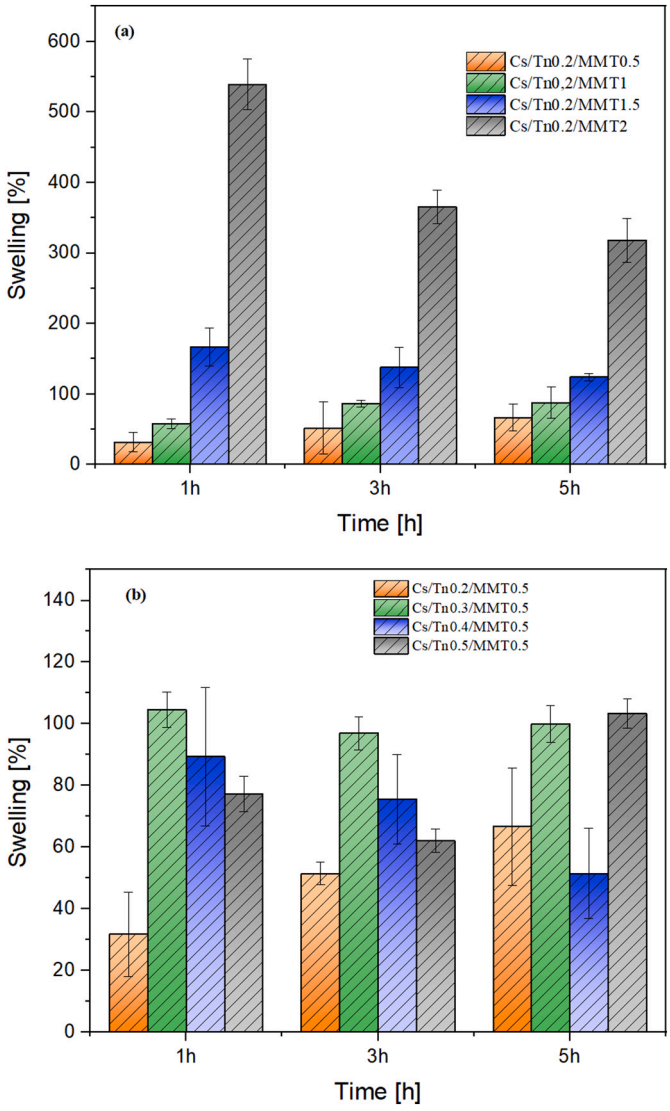

Fig. 7. Swelling percentage values of (a) Cs/Tn0.2/MMT(0.5 to 2%) films and (b) Cs/Tn(0.2 to 0.5%)/MMT0.5 films. The error bars represent standard deviations.

Table 3
Thickness measurement of the prepared films. Values are expressed as mean ± standard deviation.

Films	Thickness
Cs	0.0540 ± 0.0410
Cs/Tn0.2	0.0390 ± 0.0187
Cs/Tn0.3	0.0386 ± 0.0177
Cs/Tn0.4	0.0332 ± 0.0095
Cs/Tn0.5	0.0310 ± 0.0050
Cs/Tn0.2/MMT0.5	0.0408 ± 0.0108
Cs/Tn0.3/MMT0.5	0.0430 ± 0.0144
Cs/Tn0.4/MMT0.5	0.0408 ± 0.0113
Cs/Tn0.5/MMT0.5	0.0410 ± 0.0091
Cs/MMT0.5	0.0324 ± 0.0059
Cs/Tn0.2/MMT1	0.0420 ± 0.0192
Cs/Tn0.2/MMT1.5	0.0470 ± 0.0057
Cs/Tn0.2/MMT2	0.0542 ± 0.0149

platelet formation of MMT onto the Cs film matrix [56].

3.2. Kinetic study of MO removal

3.2.1. Effect of MO dye concentration

Three different concentrations (namely 20, 40 and 60 mg/L) were investigated to elucidate the effect of the initial MO dye concentration on the removal rate from Cs/Tn0.2/MMT0.5 film. The rest of the parameters were set at pH 7 and temperature 25 °C. On the one hand, the appearance of the films and the MO dye solution, before and after the adsorption process, are shown in Fig. 8a. The Cs/Tn0.2/MMT0.5 film was completely orange after 30 min (equilibrium time) with a concentration of 60 mg/L of MO. Accordingly, after the contact with these films, the MO dye solution presented a highly discoloured appearance. In fact, the colour of the solution became less intense after the adsorption mechanism. The same observation was reported more recently by Labidi et al., who concluded that this result is due to the presence of chelating groups on the chitosan structure [64]. On the other hand, the results related to the adsorption capacity of the films at different concentrations of MO dye are shown in Fig. 8b. It can be seen that the MO dye adsorption rate was relatively rapid, displaying an equilibrium time at 30 min for all of the MO concentrations. This result may be attributed to the large active site, present on the surface of the film [65]. Besides, the rapid equilibrium adsorption time was attributed to the many vacant adsorption sites and the quick diffusion of dye molecules to the external surface of adsorbent films. Therefore, the uptake of MO dye increased gradually from 17.20 mg/g to 53.44 mg/g, as the initial concentration increased from 20 mg/L to 60 mg/L. The increase of the initial concentration of MO tends to increase the mass transfer of dye molecules to the active sites of the adsorbents [66]. The percentage of the removal efficiency was 86% at 20 mg/L. In this respect, this work showed higher adsorption efficiency than the other studies described in the literature. Recently, Arwa and Azlan reported that the removal efficiency of MO only achieved 18.9% when a Lala clam shell was used as an adsorbent [4]. In another study, the author presented a novel kind of film, based on a magnetic maghemite/chitosan nanocomposite for methyl orange removal from aqueous solution and they found that the percentage of the adsorption only achieved 55.21% after 540 min, with 20 mg/L as the initial dye concentration [67].

Moreover, MMT and Cs were used in the films and both components are usually considered to be the most important adsorbents for MO dye removal in the literature. This could also be related to the increase in

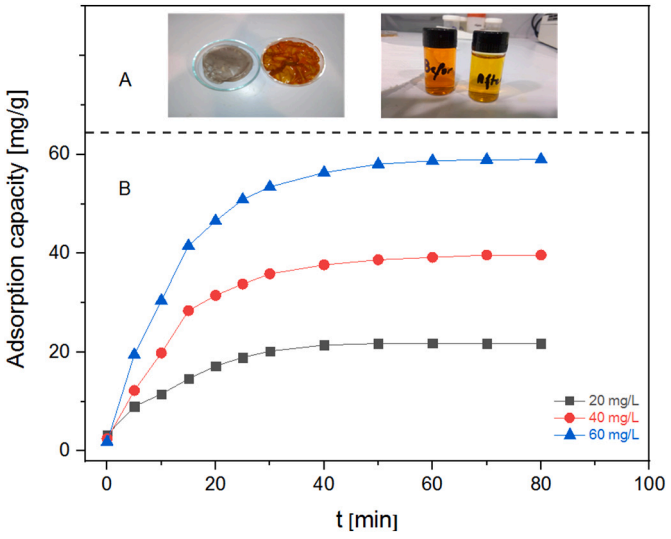

Fig. 8. (A) Films aspect before and after MO removal, (B) Variation of MO concentration removal from Cs/Tn0.2/MMT0.5 such 20, 40 and 60 mg/L at pH 7 and 25 °C.

adsorption capacity. It was reported that the presence of clay layers can improve the mechanical properties, the hydrophobicity, the thermal properties and the physical properties of the biopolymer films [68]. An electrostatic attraction can be formed between the adsorbent-adsorbate surfaces which improves the removal efficiency. This behaviour is in agreement with other published work, when tannin-immobilised cellulose hydrogels are used for the adsorption of methylene blue [69].

3.2.2. Effect of the adsorbent dose

The adsorption properties of dye depends on the specific surface and the composition of the films. For this reason, different concentrations of MMT and Tn were investigated, from 0.5% to 2.0% and from 0.2% to 0.5%, respectively. All the films were tested at 60 mg/L and the results are presented in Fig. 9. Regarding the MMT variation dose, the results showed that the adsorption capacity increased from 89.07% to 95.62%, with MMT from 0.5 to 1.0 w%. This result can be explained by the good interaction and exfoliation of MMT onto Cs/Tn films. It was reported that the negatively charged silica hydroxyl groups of clay can make hydrogen banding and ion exchange attraction with the carbonyl functional groups of biopolymers, which reinforce the matrix formation of biopolymer films [68]. Jawed et al. observed that the adsorption process of MO can include hydrogen bonding and electrostatic interaction of this anionic dye with the NH_3^+ groups present in the biofilms, based on a cross-linked chitosan structure [70].

After that, the removal efficiency decreases to 73.72%. The lowest removal rate was achieved at the highest MMT concentration (2%). This tendency could be caused by the lower porosity and hydrophilicity of Cs/Tn/MMT surfaces at higher MMT concentrations. This result may also be attributed to the saturation of the film's surface or the non-dissolution and aggregation of the MMT particles. In this sense, according to a recent study, a considerably high concentration of an adsorbent could lead to a saturation reaction of the adsorption site and the presence of particle aggregation [71].

On the other hand, the removal efficiency of MO dye was influenced by Tn concentration as well. It was observed that the removal efficiency improved slightly, with the increase of tannin percentage from 0.2 to 0.3%, because of the aromatic structure and the hydrophilic character of tannin. On the other hand, the casting process of tannin and chitosan played a fundamental role in the successful intimate interconnection between the two biopolymer-based resources. H-bonding between the surface of tannin and the polysaccharide structure of chitosan can result in contact with each other. This result was in accordance with the literature, in which tannin and cellulose polysaccharide are used as films. The authors indicate that the hydrophilic character of tannin could be the result of their adsorption into the nanocellulose matrix via H-bonding [55]. This is in accordance with previous work in the literature [69].

The adsorption of MO follows a decreasing tendency at 0.4% and, finally, an increasing trend again at 0.5% of tannin. This variation and instability of the removal efficiency may be attributed to the saturation of the films with tannin at more than 0.3% concentration. In fact, this result was in good agreement with the morphology of the films at higher tannin concentrations (decreasing the porosity, swelling and thickness of the prepared films). Nevertheless, based on these results, it can be seen that the variations observed in the removal rate were not significant. This means that the variation of the Tn concentration did not display a sufficient influence on the performance of the films toward the pollutant (MO dye).

Cs/Tn0.2/MMT1 exhibited higher adsorption capacity than the other film's formulations (57.37 mg/g corresponded to 95.62%) which may be attributed to its high porosity percentage (91.37%). The maximum adsorption capacity was considered a better fit, compared to previous works (Table 4).

3.2.3. pH depending on MO removal

The variation of pH presents another parameter with a great influence on the adsorption process. Consequently, the effect of pH variation on the removal rates was evaluated and the results are presented in Fig. 10. It was seen that, as the pH value increased from 2 to 7, the adsorption capacity of dye into Cs/Tn/MMT films increased from 50.45

Table 4
Comparison of the adsorption capacity of Cs/Tn/MMT films with other adsorbents in the literature.

Adsorbent	Initial MO concentration (mg/L)	Q_m (mg/g)	References
Fe_2O_3/chitosan films	20	28.54	[67]
Cs/MMT films	20	8.70	[85]
	40	19.50	
COMR-Clay	60–140	34.48	[86]
OMR-Clay		41.67	
Cs/Kaolin/Fe_3O_4	20	34.63	[87]
	40	75.58	
Chitosan/bentonite	50	46.67	[88]
	20	22.2	
CCG/TNC-50	40	44.4	[89]
	60	63.7	
	20	17.20	
Cs/Tn0.2/MMT0.5	40	33.80	This study
	60	53.44	
Cs/Tn0.2/MMT1	60	57.37	This study

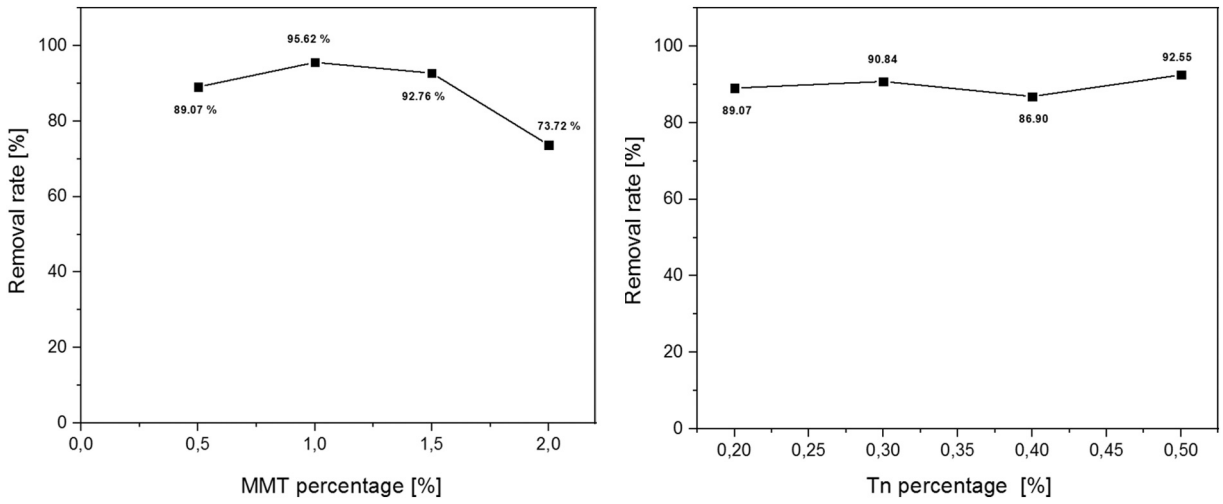

Fig. 9. Variation dose of MMT (A) and Tannin (B) amount for the removal efficiency of 60 mg/L of MO, pH 7 and 25 °C.

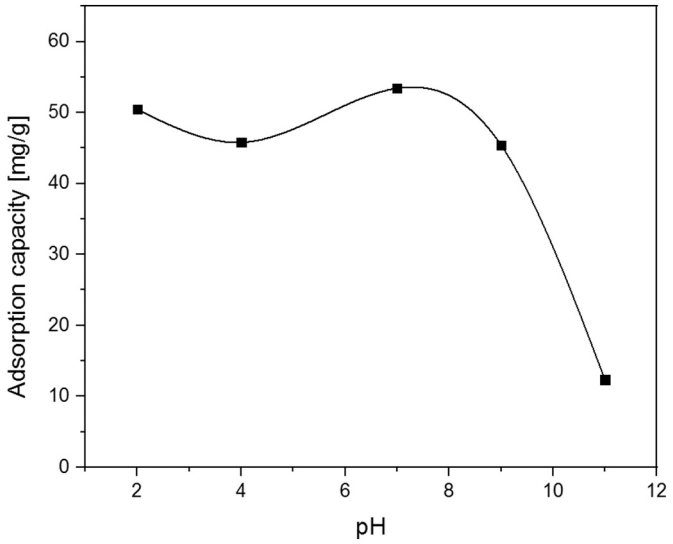

Fig. 10. pH variation of MO removal on Cs/Tn02/MMT0.5 film at 60 mg/L MO and 25 °C.

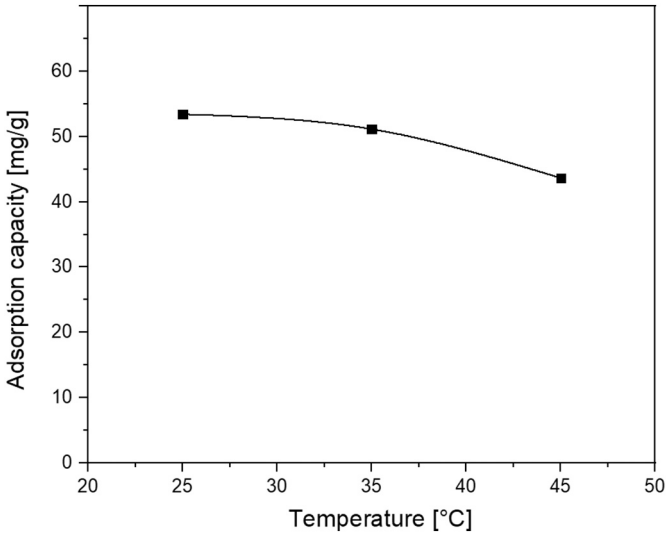

Fig. 11. The effect of temperature on the removal of MO using Cs/Tn0.2/MMT0.5 film at different temperatures (25, 35 and 45 °C) and the optimum condition.

to 53.44 mg/g. In fact, in acidic conditions, MO was protonated by H^+ in solution and this probably caused an electrostatic repulsion with the protonated adsorbent surface, resulting in a lower removal efficiency [72]. Then, as the pH increased to less acidic values, this effect was reduced and, therefore, the removal rate was enhanced. MO dye has an anionic character when the pH is above its pka value (3.3) [34]. Before this pka value (pH = 2), and when methyl orange has a cationic character, no significant difference can be achieved for the adsorption of MO (50.45 mg/g for pH 2 and 45.8 mg/g for pH 4). A similar trend was observed for the removal of MO from CSB films in the range of pH 2 to 4 [73].

The adsorption of MO displayed an optimum at pH 7 (89.07%). This anionic dye has been reported to display a naturally deprotonated cluster of functional groups, such as amino and hydroxyl groups ($MO\text{-}SO_3^-$) [74]. Accordingly, this anionic dye would be attracted to the positively charged sites present on the film surface, especially at neutral pH. A strong electrostatic interaction, n-π stacking interaction and dipole-dipole hydrogen bonding interaction can be formed between this anionic dye and the protonated adsorbent film surface. NH_3^+, the protonated silanol groups ($Si\text{-}OH_2^+$) of clay and the positively global charge surface of the Cs/Tn film enhance the adsorption mechanism of MO until the maximum is reached at pH 7 [73].

However, in alkaline conditions (pH between 9 and 11) OH^- would compete for binding to the active site of the adsorbents, decreasing the interaction adsorbent-adsorbate and, therefore, the removal efficiency. For this reason, further increments of the pH from 7 to 11 led to a reduction of the adsorption capacity, from 53.44 to 12.32 mg/g.

3.2.4. Temperature depending on MO removal and thermodynamics study

The MO removal efficiency was influenced by temperature variation in the range 25 to 45 °C onto Cs/Tn0.2/MMT0.5 film at 60 mg/L and neutral pH. The results indicated that, an increase in the temperature leads to a reduction in the adsorption capacity from 53.44 to 43.65 mg/g (Fig. 11). This result confirmed that the maximum MO removal was achieved at room temperature (25 °C), highlighting an exothermic adsorption process. The reason for this exothermic phenomenon is probably due to the weakness of the physical bonding between MO and the active sites of adsorbents at higher temperature values [65].

The thermodynamics parameters, such as Gibbs free energy ΔG°, enthalpy ΔH° and entropy ΔS°, were obtained by temperature variations at 298, 308 and 318 K and calculated according to the following equations (Eqs. (5)–(7)):

$$\Delta G^\circ = -RT\,Ln\,K_c \tag{5}$$

$$\Delta G^\circ = \Delta H^\circ - T\,\Delta S^\circ \tag{6}$$

$$Ln\,K_c = \frac{-\Delta H^\circ}{RT} + \frac{\Delta S^\circ}{R} \tag{7}$$

where R is the ideal gas constant (8.314 J/ mol K^{-1}), T is the absolute temperature and K_c is the equilibrium constant. $K_c = \frac{C_a}{C_e}$, where C_a and C_e are the adsorbent phase concentration at equilibrium and the equilibrium concentration in solution, respectively).

The calculated thermodynamic parameters are summarised in Table 5. The results indicate that ΔH° present negative values which suggested the exothermic nature of this adsorption process. The low ΔH° value pointed out that the interaction between the adsorbent surface and the adsorbate was electrostatic [75]. In addition, the negative entropy (ΔS°) value indicated the decrease in randomness at the film/dye interface during the adsorption process [67]. Furthermore, the negative value of ΔG° confirmed that the adsorption of methyl orange onto Cs/Tn0.2/MMT0.5 was feasible and thermodynamically spontaneous. It was also found that the Gibbs free energy increased from −2.728 KJ mol^{-1} K^{-1} to −1.948 KJ mol^{-1} K^{-1} when the temperature increased from 298 to 318 K, demonstrating that the removal of MO became slower and less favourable at higher temperatures. The higher affinity of MO removal toward this type of Cs/Tn0.2/MMT0.5 film was observed at lower temperatures. This result was in good agreement with the published work of Jiang Ru et al. [67].

3.2.5. Adsorption kinetic model

The mechanism of adsorption of the MO dye was modelled via the corresponding kinetic equations. They were studied according to the pseudo first-order (Eq. (8)) and the pseudo-second order (Eq. (9))

Table 5
Thermodynamic parameter of MO adsorption on Cs/Tn0.2/MMT0.5 film at 298, 308 and 318 K.

	Temperature (K)	ΔH^0	ΔS^0 (KJ mol^{-1} K^{-1})	ΔG^0
Cs/Tn0.2/MMT0.5	298	−14.350	−0.039	−2.728
	308			−2.338
	318			−1.948

models.

The pseudo-first-model was known as the Langergren kinetic model and expressed as follows:

$$log(q_e - q_t) = logq_e - k_1 t \quad (8)$$

where q_e and q_t are the adsorption capacity of each pollutant (mg/g) at equilibrium and time (t) respectively, and K_1 (1/min) is the constant adsorption of the pseudo-first-order kinetic model.

The pseudo-second-model can be expressed by the following equation:

$$\frac{1}{q_t} = \frac{1}{k_2 q_e^{\,2}} + \frac{1}{q_e}\, t \quad (9)$$

where q_t and q_e is the capacity of adsorption at time (t) and the equilibrium quantity of adsorption, respectively (mg/g), and k_2 is the equilibrium rate constant of the pseudo second order (s^{-1}).

The parameters of both models were calculated using the value of the slope and the intercept of the straight line, see Tables 6 and 7. The study was carried out based on the optimised parameters of the adsorption process discussed in the previous section (i.e. MO dye concentration, pH, temperature, dose of MMT and dose of Tn). According to the calculated values k_1, k_2 and q_e, the removal efficiency of MO through the films based on chitosan, tannin and montmorillonite was more suitable to follow the pseudo-second-order model at the same experimental conditions. The correlation coefficient (R^2) value fit the second order model better, which is closer to unity than the first order model, for all of the adsorbents. Moreover, the calculated adsorption capacity q_e with the second order model displayed a good agreement with the theoretical value. On the contrary, the theoretical and experimental values calculated with the first order model showed higher differences compared to the second order ones. The same result was described by Liu et al., who confirmed that the pseudo-second-order kinetic model was more appropriate for describing the adsorption process of MO onto A-MnO2 [65]. Wong et al. reported that the adsorption of MO onto chitosan $CaCl_2$ beads was more suitable with the pseudo second order models, indicating that the adsorption process can involve valency forces with exchange electrons between the adsorbent and adsorbate [76].

3.2.6. Adsorption isotherm

The equilibrium isotherm models of adsorption describe the phenomenon of the retention of the substance from the aqueous media in contact with a solid phase, creating a dynamic balance under equilibrium conditions [77]. A large number of models of adsorption isotherms have been developed to describe the adsorption equilibrium results, such us Langmuir, Freundlich, Temkin, Dubinin-Radushkevich etc. The Langmuir isotherm describes a monolayer adsorption model onto the homogeneous surface of an adsorbent with negligible interaction forces between adsorbed molecules [78]. The Freundlich isotherm has been developed to describe a multilayer adsorption model on a heterogeneous surface with a non-uniform adsorption distribution [79]. The Temkin isotherm assumes a linear decrease of the heat of adsorption with the increase of coverage rate, for all of the adsorbent in a layer, due to adsorbate/adsorbate interactions [80]. Finally, the Dubinin-Radushkevich (R-D) isotherm model has been employed for the adsorption onto micropore and heterogeneous surfaces, following a pore filling mechanism [81]. This approach was applied to give an idea of the physical or chemical adsorption process according to the free energy value.

These models were described as linear equations as follows (Eqs. (10)–(13)):

$$\frac{1}{Q_e} = \frac{1}{Q_m} + \frac{1}{Q_m K_L C_e} \quad (10)$$

$$logQ_e = \frac{1}{n}\, logC_e + logK_f \quad (11)$$

$$Q_e = \frac{RT}{K_T}\, lnC_e + \frac{RT}{K_T}\, lnA_T \quad (12)$$

$$lnQ_e = -K_{DR}\, \varepsilon^2 + lnQ_m \quad (13)$$

where Q_e is the adsorption capacity at equilibrium time (mg/g), C_e is the MO concentration at the equilibrium time (mg/L), Q_m is the maximum of adsorption capacity and K_L, K_F and K_T are the Langmuir, Freundlich and Temkin constants, 1/n is the Freundlich constant related to sorption capacity, n is the heterogeneity factor, A_T (L/g) is the equilibrium binding constant, K_{DR} (L/g) is the D-R isotherm constant and related to the mean free energy E (kJ/mol) given by $E = \frac{1}{(2K_{DR})^{1/2}}$ and ε is the Polanyi potential, which is equal to RT Ln (1 + 1/Ce) where R (J/mol K) is the gas constant and T (K) is the absolute temperature [82].

The parameters calculated from these isotherm models are presented in Table 8. The results indicated that the adsorption process was better described by the Langmuir and Freundlich isotherm models, since the values of the coefficient of regression R^2 were near to 1, compared to the other models. This result showed the inadequacy of the adsorption by the Temkin and Dubinin-Radushkevich (R-D) models. The 1/n value of Freundlich was <1 (0.418), which indicated the favourability of the adsorption process with this model. This was in accordance with a recent study by Somsesta et al., which demonstrated that, according to a Freundlich value, the adsorption process of methylene blue dye was favourable onto activated Carbon/cellulose films [83]. On the other hand, calculated Q_0 was less than 50 KJ/mol with the Freundlich model, which highlighted the physical adsorption process. This confirmed the results obtained with the other models. In fact, according to the DR equation, the values of adsorption energies (E) were E < 8 KJ/mol. This

Table 6
Pseudo first order model of pollutant removal for all the adsorbent at 60 mg/L, pH 7 and room temperature.

Films	Pseudo first order model			
	$Q_{e\ exp}$	$Q_{e\ cal}$	k_1	R^2
Cs/Tn0.2/ MMT0.5	53.44	16.22	0.048	0.650
Cs/Tn0.2/ MMT1	57.37	17.17	0.049	0.648
Cs/Tn0.2/ MMT1.5	55.66	18.10	0.050	0.655
Cs/Tn0.2/ MMT2	44.23	17.56	0.048	0.666
Cs/Tn0.3/ MMT0.5	54.50	13.82	0.045	0.634
Cs/Tn0.4/ MMT0.5	52.14	12.61	0.044	0.623
Cs/Tn0.5/ MMT0.5	55.53	13.36	0.045	0.625

Table 7
Pseudo second order model of pollutant removal for all the adsorbent at 60 mg/L, pH 7 and room temperature.

Films	Pseudo second order model			
	$Q_{e\ exp}$	$Q_{e\ cal}$	k_2 (10^{-3})	R^2
Cs/Tn0.2/MMT0.5	53.44	64.93	2.1	0.9875
Cs/Tn0.2/MMT1	57.37	64.51	2.8	0.9890
Cs/Tn0.2/MMT1.5	55.66	65.78	2.2	0.9872
Cs/Tn0.2/MMT2	44.23	78.12	0.5	0.9025
Cs/Tn0.3/MMT0.5	54.50	58.82	4.9	0.9956
Cs/Tn0.4/MMT0.5	52.14	60.24	3.4	0.9945
Cs/Tn0.5/MMT0.5	55.53	60.24	4.8	0.9960

Table 8
Langmuir, Freundlich, Temkin and Dubinin isotherms models for MO removing.

	R^2	K (Isotherm cst)	Energy (KJ/mol)	Qm (mg/g)
Langmuir	0.942	0.537	–	52.88
Freundlich	0.936	18.063	5.932	–
Temkin	0.851	192.9	0.013	–
Duninin-Radushkevich	0.847	310	1.200	42.88

result suggested that the adsorption occurred because of the physical nature of the adsorbents [27]. Considering the coefficient of regression, the Langmuir model produced the best correlation, which presented higher values than the Freundlich isotherm model [67]. This result suggested that the adsorption of MO onto Cs/Tn/MMT followed a homogeneous distribution and monolayer film surface. The value of the maximum adsorption capacity was 52.88 mg/g with the Langmuir isotherm, which was close to the experimental data. According to a recent study, Reactive Black 5 dye removal from the vanadium/chitosan film was more suitable with the Langmuir isotherm model as well [75]. In this respect, the structure of cellulose/chitosan composite films has been studied recently, to prove the better fitting of the Langmuir model and indicating a monolayer coverage of congo red removal [84].

4. Conclusion

This work has demonstrated the effectiveness of different Cs/Tn/MMT film formulations for methyl orange removal from aqueous solution. Firstly, it was seen that the content of the different compounds in the film formulations significantly influenced their properties and structure. The integration of the tannins and montmorillonite in the chitosan matrix provided a synergistic effect and enhanced the performance. The experimental findings showed that initial dye concentration, adsorbent concentration, pH solution and temperature all had a significant effect on the uptake capacities of the adsorbent. In this respect, the films displayed optimal conditions of adsorption at 60 mg/L, as the initial MO concentration, pH =7 and 25 °C, which were recorded at an equilibrium time of 30 min. Cs/Tn0.2/MMT1 exhibited a relatively higher adsorption capacity (57.37 mg/g, corresponding to 95.62%) with respect to the other film formulation. The thermodynamic study suggested that the adsorption process was thermodynamically spontaneous, exothermic and presented a decrease of randomness in the adsorbent-adsorbate interface. Furthermore, the adsorption of MO followed a pseudo second order rate equation and fitted the homogeneous and monolayer Langmuir isotherm with good correlation. Thus, Cs/Tn/MMT films could have an appropriate potential for waste water treatment.

CRediT authorship contribution statement

Nadia Tahari: Investigation, Conceptualization, Methodology, Writing – original draft. **Pedro L. de Hoyos-Martinez:** Formal analysis, Writing – original draft. **Nagore Izaguirre:** Formal analysis, Visualization. **Nefzi Houwaida:** Visualization, Writing – original draft. **Manef Abderrabba:** Supervision. **Sameh Ayadi:** Supervision, Validation. **Jalel Labidi:** Resources, Funding acquisition, Writing – review & editing.

Acknowledgements

The authors thank the Basque Government (IT1008-16) and Tunis El Manar University for financially supporting this work.

References

[1] S.K. Panda, I. Aggarwal, H. Kumar, L. Prasad, A. Kumar, A. Sharma, D.N. Vo, D. Van Thuan, V. Mishra, Magnetite Nanoparticles as Sorbents for Dye Removal: A Review, Springer International Publishing, 2021, https://doi.org/10.1007/s10311-020-01173-9.

[2] Y. Tang, R. Yang, D. Ma, B. Zhou, L. Zhu, J. Yang, Removal of methyl orange from aqueous solution by adsorption onto a hydrogel composite, Polym. Polym. Compos. 26 (2018) 161–168, https://doi.org/10.1177/096739111802600204.

[3] E. Bazrafshan, A.A. Zarei, H. Nadi, M.A. Zazouli, Adsorptive Removal of Methyl Orange and Reactive Red 198 dyes by Moringa Peregrina Ash vol. 21, 2014, pp. 105–113.

[4] A. Alseddig, A. Eljiedi, A. Kamari, Removal of methyl orange and methylene blue dyes from aqueous solution using lala clam (Orbicularia orbiculata), Shell 040003 (2017), https://doi.org/10.1063/1.4983899.

[5] J.E. Aguiar, J.A. Cecilia, P.A.S. Tavares, D.C.S. Azevedo, E.R. Castellón, S.M. P. Lucena, I.J.S. Junior, Applied clay science adsorption study of reactive dyes onto porous clay heterostructures, Appl. Clay Sci. (2016) 1–10, https://doi.org/10.1016/j.clay.2016.09.001.

[6] A.E. Blum, D.D. Eberl, Measurement of clay surface areas by polyvinylpyrrolidone (PVP) sorption and its use for quantifying illite and smectite abundance, Clays Clay Miner. 52 (2004) 589–602, https://doi.org/10.1346/CCMN.2004.0520505.

[7] N. Tahari, P.L. de Hoyos-Martinez, M. Abderrabba, S. Ayadi, J. Labidi, Lignin - montmorillonite hydrogels as toluene adsorbent, Colloids Surfaces A Physicochem. Eng. Asp. 602 (2020), 125108, https://doi.org/10.1016/j.colsurfa.2020.125108.

[8] A.H. Jawad, A.S. Abdulhameed, E. Kashi, Z.M. Yaseen, Z.A. ALOthman, M.R. Khan, Cross-linked chitosan-Glyoxal/kaolin clay composite: parametric optimization for color removal and COD reduction of remazol brilliant blue R dye, J. Polym. Environ. (2021), https://doi.org/10.1007/s10924-021-02188-1.

[9] N.N. Bahrudin, M.A. Nawi, A.H. Jawad, S. Sabar, Adsorption characteristics and mechanistic study of immobilized chitosan-montmorillonite composite for methyl orange removal, J. Polym. Environ. 28 (2020) 1901–1913, https://doi.org/10.1007/s10924-020-01734-7.

[10] A.H. Jawad, A.S. Abdulhameed, N.N.A. Malek, Z.A. ALOthman, Statistical optimization and modeling for color removal and COD reduction of reactive blue 19 dye by mesoporous chitosan-epichlorohydrin/kaolin clay composite, Int. J. Biol. Macromol. 164 (2020) 4218–4230, https://doi.org/10.1016/j.ijbiomac.2020.08.201.

[11] Z. Yin, S. Li, D. Hu, Z. Li, R. Chu, C. Liu, X. Li, J. Hu, L. Zhu, Performance evaluation of different chitosan-clay composite materials for efficient harvesting of Chlorella vulgaris and impacts on downstream bioproduct processing and water reusability, Chem. Eng. J. 430 (2022), https://doi.org/10.1016/j.cej.2021.132892.

[12] J.H.R. Llanos, L. Avezum, G.C. Dacanal, C.C. Tadini, Increase in the physical performance of nanostructured starch/chitosan blends with montmorillonite, Colloid Polym. Sci. 299 (2021) 1901–1915, https://doi.org/10.1007/s00396-021-04907-5.

[13] J. Janesch, M. Jones, M. Bacher, E. Kontturi, A. Bismarck, A. Mautner, Mushroom-derived chitosan-glucan nanopaper filters for the treatment of water, React. Funct. Polym. (2019), 104428, https://doi.org/10.1016/j.reactfunctpolym.2019.104428.

[14] A.H. Jawad, A. Islam, B.H. Hameed, International Journal of Biological Macromolecules Cross-linked chitosan thin film coated onto glass plate as an effective adsorbent for adsorption of reactive orange 16, Int. J. Biol. Macromol. 95 (2017) 743–749, https://doi.org/10.1016/j.ijbiomac.2016.11.087.

[15] A. Sionkowska, M. Michalska-sionkowska, M. Walczak, International Journal of Biological Macromolecules Preparation and characterization of collagen / hyaluronic acid / chitosan fi lm crosslinked with dialdehyde starch, Int. J. Biol. Macromol. 149 (2020) 290–295, https://doi.org/10.1016/j.ijbiomac.2020.01.262.

[16] M. Rodríguez-vázquez, B. Vega-ruiz, R. Ramos-zúñiga, D.A. Saldaña-koppel, L. F. Quiñones-olvera, Chitosan and its potential use as a scaffold for tissue engineering in regenerative medicine, Biomed. Res. Int. 2015 (2015) 1–15, https://doi.org/10.1155/2015/821279.

[17] P.L. Kashyap, X. Xiang, P. Heiden, Chitosan nanoparticle based delivery systems for sustainable agriculture, Int. J. Biol. Macromol. 77 (2015) 36–51, https://doi.org/10.1016/j.ijbiomac.2015.02.039.

[18] A. Duran, H.I. Kahve, The effect of chitosan coating and vacuum packaging on the microbiological and chemical properties of beef, Meat Sci. 162 (2020), 107961, https://doi.org/10.1016/j.meatsci.2019.107961.

[19] A.H. Jawad, A.S. Abdulhameed, Facile synthesis of crosslinked chitosan-tripolyphosphate/kaolin clay composite for decolourization and COD reduction of remazol brilliant blue R dye: optimization by using response surface methodology, Colloids Surfaces A Physicochem. Eng. Asp. 605 (2020), 125329, https://doi.org/10.1016/j.colsurfa.2020.125329.

[20] W. Li, Y. Tang, Y. Zeng, Z. Tong, D. Liang, W. Cui, Adsorption behavior of Cr(VI) ions on tannin-immobilized activated clay, Chem. Eng. J. 193–194 (2012) 88–95, https://doi.org/10.1016/j.cej.2012.03.084.

[21] G. Amaral-Labat, L.I. Grishechko, V. Fierro, B.N. Kuznetsov, A. Pizzi, A. Celzard, Tannin-based xerogels with distinctive porous structures, Biomass Bioenergy 56 (2013) 437–445, https://doi.org/10.1016/j.biombioe.2013.06.001.

[22] J. Sánchez-Martín, J. Beltrán-Heredia, P. Gibello-Pérez, Adsorbent biopolymers from tannin extracts for water treatment, Chem. Eng. J. J. 168 (2011) 1241–1247, https://doi.org/10.1016/j.cej.2011.02.022.

[23] E. Binaeian, N. Seghatoleslami, M.J. Chaichi, Synthesis of oak gall tannin-immobilized hexagonal mesoporous silicate (OGT-HMS) as a new super adsorbent for the removal of anionic dye from aqueous solution, Desalin. Water Treat. 57 (2016) 8420–8436, https://doi.org/10.1080/19443994.2015.1020513.

[24] T.S. Anirudhan, P.S. Suchithra, Synthesis and characterization of tannin-immobilized hydrotalcite as a potential adsorbent of heavy metal ions in effluent treatments, Appl. Clay Sci. 42 (2008) 214–223, https://doi.org/10.1016/j.clay.2007.12.002.

[25] H. Sun, N. Xia, Z. Liu, F. Kong, S. Wang, Chemosphere removal of copper and cadmium ions from alkaline solutions using chitosan-tannin functional paper materials as adsorbent, Chemosphere. 236 (2019), 124370, https://doi.org/10.1016/j.chemosphere.2019.124370.

[26] X. Qiu, S. Zhao, Adsorption of RE 3 + from aqueous solutions by bayberry tannin immobilized on chitosan, Environ. Technol. 0 (2017) 1–8, https://doi.org/10.1080/09593330.2017.1384072.

[27] N. Akter, A. Hossain, M.J. Hassan, M.K. Amin, M. Elias, M.M. Rahman, A.M. Asiri, I.A. Siddiquey, M.A. Hasnat, Journal of environmental chemical engineering amine modified tannin gel for adsorptive removal of brilliant green dye, Biochem. Pharmacol. 4 (2016) 1231–1241, https://doi.org/10.1016/j.jece.2016.01.013.

[28] M. Vakili, M. Rafatullah, B. Salamatinia, A. Zuhairi, M. Hakimi, K. Bing, Z. Gholami, P. Amouzgar, Application of chitosan and its derivatives as adsorbents for dye removal from water and wastewater: a review, Carbohydr. Polym. 113 (2014) 115–130, https://doi.org/10.1016/j.carbpol.2014.07.007.

[29] H. Choi, S. Yu, Application of novel hybrid bioadsorbent, tannin/chitosan/sericite, for the removal of Pb (II) toxic ion from aqueous solution, Korean J. Chem. Eng. 35 (2018) 1–9, https://doi.org/10.1007/s11814-018-0140-7.
[30] Z. Wang, P. Fang, P. Kumar, W. Wang, B. Liu, J. Li, Controlled growth of LDH films with enhanced photocatalytic activity in a mixed wastewater treatment, Nanomaterials 9 (2019), https://doi.org/10.3390/nano9060807.
[31] T.V. Rêgo, T.R.S. Cadaval, G.L. Dotto, L.A.A. Pinto, Statistical optimization, interaction analysis and desorption studies for the azo dyes adsorption onto chitosan films, J. Colloid Interface Sci. 411 (2013) 27–33, https://doi.org/10.1016/j.jcis.2013.08.051.
[32] M.R. Lasheen, I.Y. El-Sherif, M.E. Tawfik, S.T. El-Wakeel, M.F. El-Shahat, Preparation and adsorption properties of nano magnetite chitosan films for heavy metal ions from aqueous solution, Mater. Res. Bull. 80 (2016) 344–350, https://doi.org/10.1016/j.materresbull.2016.04.011.
[33] B. Barik, P.S. Nayak, L.S.K. Achary, A. Kumar, P. Dash, Synthesis of alumina-based cross-linked chitosan-HPMC biocomposite film: an efficient and user-friendly adsorbent for multipurpose water purification, New J. Chem. 44 (2019) 322–337, https://doi.org/10.1039/c9nj03945g.
[34] N.S. Abdul Mubarak, T.W. Chuan, H.P. Khor, A.H. Jawad, L.D. Wilson, S. Sabar, Immobilized Fe-loaded chitosan film for methyl orange dye removal: competitive ions, reusability, and mechanism, J. Polym. Environ. 29 (2021) 1050–1062, https://doi.org/10.1007/s10924-020-01949-8.
[35] L. Laysandra, I.J. Ondang, Y. Ju, B.H. Ariandini, A. Mariska, F.E. Soetaredjo, J. N. Putro, S.P. Santoso, F.L. Darsono, Highly adsorptive chitosan / saponin-bentonite composite film for removal of methyl orange and Cr (VI), Environ. Sci. Pollut. Res. 26 (2019) 5020–5037, https://doi.org/10.1007/s11356-018-4035-2.
[36] V.M. Hernandez-Izquierdo, J.M. Krochta, Thermoplastic processing of proteins for film formation - a review, J. Food Sci. 73 (2008) 30–39, https://doi.org/10.1111/j.1750-3841.2007.00636.x.
[37] J.P. Zhang, A.Q. Wang, Synergistic effects of Na +−montmorillonite and multi-walled carbon nanotubes on mechanical properties of chitosan film, Express Polym Lett 3 (2009) 302–308, https://doi.org/10.3144/expresspolymlett.2009.38.
[38] M. Shahbazi, G. Rajabzadeh, S.J. Ahmadi, Characterization of nanocomposite film based on chitosan intercalated in clay platelets by electron beam irradiation, Carbohydr. Polym. 157 (2017) 226–235, https://doi.org/10.1016/j.carbpol.2016.09.018.
[39] J. Dutta, N. Devi, Preparation, optimization, and characterization of chitosan-sepiolite nanocomposite films for wound healing, Int. J. Biol. Macromol. 186 (2021) 244–254, https://doi.org/10.1016/j.ijbiomac.2021.07.020.
[40] N. Devi, J. Dutta, Preparation and characterization of chitosan-bentonite nanocomposite films for wound healing application, Int. J. Biol. Macromol. 104 (2017) 1897–1904, https://doi.org/10.1016/j.ijbiomac.2017.02.080.
[41] N. Devi, J. Dutta, Development and in vitro characterization of chitosan/starch/halloysite nanotubes ternary nanocomposite films, Int. J. Biol. Macromol. 127 (2019) 222–231, https://doi.org/10.1016/j.ijbiomac.2019.01.047.
[42] M. Salari, M. Sowti Khiabani, R. Rezaei Mokarram, B. Ghanbarzadeh, H. Samadi Kafil, Development and evaluation of chitosan based active nanocomposite films containing bacterial cellulose nanocrystals and silver nanoparticles, Food Hydrocoll. 84 (2018) 414–423, https://doi.org/10.1016/j.foodhyd.2018.05.037.
[43] G. Hao, Y. Hu, L. Shi, J. Chen, A. Cui, W. Weng, K. Osako, Physicochemical characteristics of chitosan from swimming crab (Portunus trituberculatus) shells prepared by subcritical water pretreatment, Sci. Rep. 11 (2021) 1–9, https://doi.org/10.1038/s41598-021-81318-0.
[44] W. Lan, S. Wang, Z. Zhang, X. Liang, X. Liu, J. Zhang, Development of red apple pomace extract/chitosan-based films reinforced by TiO2 nanoparticles as a multifunctional packaging material, Int. J. Biol. Macromol. 168 (2021) 105–115, https://doi.org/10.1016/j.ijbiomac.2020.12.051.
[45] V. Rubentheren, T.A. Ward, C.Y. Chee, P. Nair, Physical and chemical reinforcement of chitosan film using nanocrystalline cellulose and tannic acid, Cellulose 22 (2015) 2529–2541, https://doi.org/10.1007/s10570-015-0650-y.
[46] C. Peña, K. de la Caba, A. Eceiza, R. Ruseckaite, I. Mondragon, Enhancing water repellence and mechanical properties of gelatin films by tannin addition, Bioresour. Technol. 101 (2010) 6836–6842, https://doi.org/10.1016/j.biortech.2010.03.112.
[47] A. Marsh, A. Heath, P. Patureau, M. Evernden, P. Walker, Alkali activation behaviour of un-calcined montmorillonite and illite clay minerals, Appl. Clay Sci. 166 (2018) 250–261, https://doi.org/10.1016/j.clay.2018.09.011.
[48] Z. Wang, H. Kang, W. Zhang, S. Zhang, J. Li, Improvement of interfacial interactions using natural polyphenol-inspired tannic acid-coated nanoclay enhancement of soy protein isolate biofilms, Appl. Surf. Sci. 401 (2017) 271–282, https://doi.org/10.1016/j.apsusc.2017.01.015.
[49] A.B. Reddy, B. Manjula, T. Jayaramudu, E.R. Sadiku, P. Anand Babu, S. Periyar Selvam, 5-fluorouracil loaded chitosan–PVA/Na+MMT nanocomposite films for drug release and antimicrobial activity, Nano-Micro Lett. 8 (2016) 260–269, https://doi.org/10.1007/s40820-016-0086-4.
[50] C.H. Zhou, Z.F. Shen, L.H. Liu, S.M. Liu, Preparation and functionality of clay-containing films, J. Mater. Chem. 21 (2011) 15132–15153, https://doi.org/10.1039/c1jm11479d.
[51] T. Ward, V. Rubentheren, T.A. Ward, C.Y. Chee, P. Nair, E. Salami, C. Fearday, Effects of heat treatment on chitosan nanocomposite film reinforced with nanocrystalline cellulose and tannic acid effects of heat treatment on chitosan nanocomposite film reinforced with nanocrystalline cellulose and tannic acid, Carbohydr. Polym. 140 (2015) 202–208, https://doi.org/10.1016/j.carbpol.2015.12.068.
[52] A.M. Shehap, R.A. Nasr, M.A. Mahfouz, A.M. Ismail, Preparation and characterizations of high doping chitosan/MMT nanocomposites films for removing iron from ground water, J. Environ. Chem. Eng. 9 (2021), 104700, https://doi.org/10.1016/j.jece.2020.104700.
[53] M. Thébault, A. Pizzi, S. Abdalla, Isocyanate-free polyurethanes by coreaction of condensed tannins with aminated tannins, J. Renew. Mater. 5 (2017) 21–29, https://doi.org/10.7569/JRM.2016.634116.
[54] X. Sun, Y. Hao, Y. Cao, Q. Zeng, Superadsorbent hydrogel based on lignin and montmorillonite for Cu (II) ions removal from aqueous solution, Int. J. Biol. Macromol. 127 (2019) 511–519, https://doi.org/10.1016/j.ijbiomac.2019.01.058.
[55] W. Zhang, Y. Ma, C. Wang, S. Li, M. Zhang, F. Chu, Preparation and properties of lignin-phenol-formaldehyde resins based on different biorefinery residues of agricultural biomass, Ind. Crop. Prod. 43 (2013) 326–333, https://doi.org/10.1016/j.indcrop.2012.07.037.
[56] D. Enescu, C. Gardrat, H. Cramail, C. Le Coz, G. Sèbe, V. Coma, Bio-inspired films based on chitosan, nanoclays and cellulose nanocrystals: structuring and properties improvement by using water-evaporation-induced self-assembly, Cellulose 26 (2019) 2389–2401, https://doi.org/10.1007/s10570-018-2211-7.
[57] S. Rivero, M.A. García, A. Pinotti, Physical and chemical treatments on chitosan matrix to modify film properties and kinetics of biodegradation, J. Mater. Phys. Chem. 1 (2013) 51–57, https://doi.org/10.12691/jmpc-1-3-5.
[58] O. Orliac, A. Rouilly, F. Silvestre, L. Rigal, Effects of additives on the mechanical properties, hydrophobicity and water uptake of thermo-moulded films produced from sunflower protein isolate, Polymer (Guildf) 43 (2002) 5417–5425, https://doi.org/10.1016/S0032-3861(02)00434-2.
[59] H. Wang, L. Wang, Developing a bio-based packaging fi lm from soya by-products incorporated with valonea tannin, J. Clean. Prod. (2017) 1–10, https://doi.org/10.1016/j.jclepro.2016.12.064.
[60] P. Chen, X. Fengwei, T. McNally, Understanding the effects of montmorillonite and sepiolite on the properties of solution-cast chitosan and chitosan / silk peptide composite films, Polym. Int. (2020), https://doi.org/10.1002/pi.6103.
[61] P. Li, J.A. Sirviö, A. Haapala, A. Khakalo, H. Liimatainen, Anti-oxidative and UV-absorbing biohybrid film of cellulose nanofibrils and tannin extract, Food Hydrocoll. 92 (2019) 208–217, https://doi.org/10.1016/j.foodhyd.2019.02.002.
[62] R. Cu, J. Yan, J. Cao, Y. Qin, M. Yuan, L. Li, Release properties of cinnamaldehyde loaded by montmorillonite in chitosan-based antibacterial food packaging, Int. J. Food Sci. Technol. 31 (2020), https://doi.org/10.1111/ijfs.14912.
[63] Y. Kasirga, A. Oral, C. Caner, Preparation and Characterization of Chitosan / Montmorillonite-K10 Nanocomposites Films for Food Packaging Applications, 2012, https://doi.org/10.1002/pc.22310.
[64] A. Labidi, A.M. Salaberria, S.C.M. Fernandes, J. Labidi, M. Abderrabba, Functional chitosan derivative and chitin as decolorization materials for methylene blue and methyl orange from aqueous solution, Materials (Basel) 12 (2019), https://doi.org/10.3390/ma12030361.
[65] Y. Liu, J. Wei, Y. Tian, S. Yan, The structure-property relationship of manganese oxides: highly efficient removal of methyl orange from aqueous solution, J. Mater. Chem. A 3 (2015) 19000–19010, https://doi.org/10.1039/c5ta05507e.
[66] V.L. Wong, S.Y. Tay, L.S. S, Enhanced removal of Methyl Orange from aqueous solution by chitosan-CaCl2 beads, Mater. Sci. Eng. 736 (2020) 1–13, https://doi.org/10.1088/1757-899X/736/2/022049.
[67] R. Jiang, Y.Q. Fu, H.Y. Zhu, J. Yao, L. Xiao, Removal of methyl orange from aqueous solutions by magnetic maghemite/chitosan nanocomposite films: adsorption kinetics and equilibrium, J. Appl. Polym. Sci. 125 (2012), https://doi.org/10.1002/app.37003.
[68] J.T. Martins, A.I. Bourbon, A.C. Pinheiro, B.W.S. Souza, M.A. Cerqueira, A. A. Vicente, Biocomposite films based on κ-carrageenan/locust bean gum blends and clays: physical and antimicrobial properties, Food Bioprocess Technol. 6 (2013) 2081–2092, https://doi.org/10.1007/s11947-012-0851-4.
[69] Y. Pei, S. Chu, Y. Chen, Z. Li, J. Zhao, S. Liu, X. Wu, J. Liu, X. Zheng, K. Tang, Full paper tannin-immobilized cellulose hydrogel fabricated by a homogeneous reaction as a potential adsorbent for removing cationic organic dye from aqueous solution, Int. J. Biol. Macromol. (2017), https://doi.org/10.1016/j.ijbiomac.2017.05.072.
[70] A.H. Jawad, N.F.H. Mamat, B.H. Hameed, K. Ismail, Biofilm of cross-linked chitosan-ethylene glycol diglycidyl ether for removal of reactive red 120 and methyl orange: adsorption and mechanism studies, J. Environ. Chem. Eng. 7 (2019), 102965, https://doi.org/10.1016/j.jece.2019.102965.
[71] R. Akhbarizadeh, F. Moore, D. Mowla, B. Keshavarzi, Improved waste-sourced biocomposite for simultaneous removal of crude oil and heavy metals from synthetic and real oilfield-produced water, Environ. Sci. Pollut. Res. 25 (2018) 31407–31420, https://doi.org/10.1007/s11356-018-3136-2.
[72] M. Mobarak, A.Q. Selim, E.A. Mohamed, M.K. Seliem, A superior adsorbent of CTAB/H2O2 solution−modified organic carbon rich-clay for hexavalent chromium and methyl orange uptake from solutions, J. Mol. Liq. 259 (2018) 384–397, https://doi.org/10.1016/j.molliq.2018.02.014.
[73] S. Ismadji, L. Laysandra, Highly adsorptive chitosan / saponin- bentonite composite film for removal of methyl orange and Cr (VI related papers), Environ. Sci. Pollut. Res. 26 (2019) 5020–5037, https://doi.org/10.1007/s11356-018-4035-2.
[74] J.C.M. Caje, P.M. de Oliveira, F.S. Semaan, R.C. Cruz, R.J. Cassella, W.F. Pacheco, Sorption properties of methyl orange onto chemically modified chitosan: thermodynamics and kinetics studies, SM Anal. Bioanal. Tech. 2 (2017) 1–9, https://doi.org/10.36876/smabt.1006.
[75] D.A.S. Rodrigues, J.M. Moura, G.L. Dotto, T.R.S. Cadaval, L.A.A. Pinto, Preparation, characterization and dye adsorption/reuse of chitosan-vanadate films, J. Polym. Environ. 26 (2018) 2917–2924, https://doi.org/10.1007/s10924-017-1171-6.

[76] V.L. Wong, S.Y. Tay, S.S. Lim, Enhanced removal of methyl orange from aqueous solution by chitosan-CaCl2 beads, IOP Conf. Ser. Mater. Sci. Eng. 736 (2020), https://doi.org/10.1088/1757-899X/736/2/022049.
[77] K.Y. Foo, B.H. Hameed, Insights into the modeling of adsorption isotherm systems, Chem. Eng. J. 156 (2010) 2–10, https://doi.org/10.1016/j.cej.2009.09.013.
[78] I. Langmuir, The constitution and fundamental properties of solids and liquids. Part II.-liquids, J. Frankl. Inst. 184 (1917) 721, https://doi.org/10.1016/s0016-0032(17)90088-2.
[79] H. Freundlich, Over the Adsorption in Solution 57, 1906, pp. 385–471, https://doi.org/10.1515/zpch-1907-5723.
[80] M.I. Temkin, Kinetics of ammonia Synthesis on Promoted iron Catalyst, 1991.
[81] M.M. Dubinin, Fundamentals of the theory of adsorption in micropores of carbon adsorbents: characteristics of their adsorption properties and microporous structures, Carbon N. Y. 27 (1989) 457–467, https://doi.org/10.1016/0008-6223(89)90078-X.
[82] D. Balarak, F. Mostafapour, H. Azarpira, A. Joghataei, Langmuir, Freundlich, Temkin and Dubinin–radushkevich isotherms studies of equilibrium sorption of ampicilin unto montmorillonite nanoparticles, J. Pharm. Res. Int. 20 (2017) 1–9, https://doi.org/10.9734/jpri/2017/38056.
[83] N. Somsesta, V. Sricharoenchaikul, D. Aht-Ong, Adsorption removal of methylene blue onto activated carbon/cellulose biocomposite films: equilibrium and kinetic studies, Mater. Chem. Phys. 240 (2020), 122221, https://doi.org/10.1016/j.matchemphys.2019.122221.
[84] X. Zheng, X. Li, J. Li, L. Wang, W. Jin, J. Liu, Y. Pei, K. Tang, Efficient removal of anionic dye (Congo red) by dialdehyde microfibrillated cellulose/chitosan composite film with significantly improved stability in dye solution, Int. J. Biol. Macromol. 107 (2018) 283–289, https://doi.org/10.1016/j.ijbiomac.2017.08.169.
[85] N.N. Bahrudin, M.A. Nawi, S. Sabar, Immobilized chitosan-montmorillonite composite adsorbent and its photocatalytic regeneration for the removal of methyl orange, React. Kinet. Mech. Catal. 126 (2019) 1135–1153, https://doi.org/10.1007/s11144-019-01536-6.
[86] A.M. Zayed, M.S.M. Abdel Wahed, E.A. Mohamed, M. Sillanpää, Insights on the role of organic matters of some Egyptian clays in methyl orange adsorption: isotherm and kinetic studies, Appl. Clay Sci. 166 (2018) 49–60, https://doi.org/10.1016/j.clay.2018.09.013.
[87] D.M. Liu, C. Dong, J. Zhong, S. Ren, Y. Chen, T. Qiu, Facile preparation of chitosan modified magnetic kaolin by one-pot coprecipitation method for efficient removal of methyl orange, Carbohydr. Polym. 245 (2020), 116572, https://doi.org/10.1016/j.carbpol.2020.116572.
[88] L. Zhang, Q. Liu, P. Hu, R. Huang, Adsorptive removal of methyl orange using enhanced cross-linked chitosan/bentonite composite, Desalin. Water Treat. 57 (2016) 17011–17022, https://doi.org/10.1080/19443994.2015.1088478.
[89] A.K.T. Mohammad, A.S. Abdulhameed, A.H. Jawad, Box-Behnken design to optimize the synthesis of new crosslinked chitosan-glyoxal/TiO 2 nanocomposite: methyl orange adsorption and mechanism studies, Int. J. Biol. Macromol. 129 (2019) 98–109, https://doi.org/10.1016/j.ijbiomac.2019.02.025.